

Space Weather

RESEARCH ARTICLE

10.1029/2020SW002536

Key Points:

- Occurrence rates of ionospheric scintillation indices at high latitudes during two years from a single station are statistically analyzed
- Occurrence rates of phase scintillation index strongly depend on the signal frequency, geomagnetic activity, season, and magnetic local time
- Polar cap patch, polar cusp, field-aligned currents, and auroral oval are strongly related to the climatology of phase scintillation index

Correspondence to:

J.-K. Chung,
jkchung@kasi.re.kr

Citation:

Hong, J., Chung, J.-K., Kim, Y. H., Park, J., Kwon, H.-J., Kim, J.-H., et al. (2020). Characteristics of ionospheric irregularities using GNSS scintillation indices measured at Jang Bogo Station, Antarctica (74.62°S, 164.22°E). *Space Weather*, 18, e2020SW002536. <https://doi.org/10.1029/2020SW002536>

Received 7 MAY 2020

Accepted 29 SEP 2020

Accepted article online 5 OCT 2020

Characteristics of Ionospheric Irregularities Using GNSS Scintillation Indices Measured at Jang Bogo Station, Antarctica (74.62°S, 164.22°E)

Junseok Hong¹ , Jong-Kyun Chung¹ , Yong Ha Kim² , Jaeheung Park^{1,3} , Hyuck-Jin Kwon⁴, Jeong-Han Kim⁴ , Jong-Min Choi⁵ , and Young-Sil Kwak^{1,3} 

¹Space Science Division, Korea Astronomy and Space Science Institute, Daejeon, South Korea, ²Department of Astronomy, Space Science and Geology, Chungnam National University, Daejeon, South Korea, ³Department of Astronomy and Space Science, Korea University of Science and Technology, Daejeon, South Korea, ⁴Division of Polar Climate Sciences, Korea Polar Research Institute, Incheon, South Korea, ⁵Department of Earth Sciences, National Cheng Kung University, Tainan, Taiwan

Abstract Global Navigation Satellite System (GNSS) signals strongly depend on the ionospheric conditions, which are composed of electrons and ions generated by solar radiation and particle precipitation. Ionospheric plasma irregularities may cause the scintillation of the GNSS signals or even the loss of signal lock, resulting in the reduction of positioning accuracy and timing precision. Phase scintillation phenomenon is known to occur frequently at high latitudes and primarily related to a significant plasma density gradient, which is due to fast plasma flows in the polar region, energetic particle precipitation in the auroral region, polar cap patches, or several instability mechanisms. Statistical studies are required to understand the characteristics of ionospheric (both phase and amplitude) scintillations at high latitudes. Here, we report the results of ionospheric scintillation measurements at Jang Bogo Station (JBS; 74.62°S, 164.22°E), located inside the polar cap region in Antarctica. The occurrence rates of ionospheric scintillations over the JBS are recorded for 2 years (2017–2018) during solar minimum conditions. The occurrence rates of amplitude scintillations increase only at lower elevation angles (below 30°), which are hard to determine whether the source is ionospheric irregularity or ambient noise such as multipath. In contrast, the occurrence rates of phase scintillations depend on the azimuth angle, season, magnetic activity, magnetic local time, and signal frequency. The results of our analysis suggest that users of the GNSS should consider these parameters to prepare for the degradation of the GNSS performance at high latitudes in the Southern Hemisphere.

1. Introduction

The ionosphere is composed of electrons and ions, which are mainly photoionized by solar radiation. Ionospheric plasma can affect transionospheric radio waves such as Global Navigation Satellite System (GNSS) signals. Especially, the ionospheric irregular plasma density causes the fluctuation of the signal strength or signal phase differences between satellites and receivers (Aarons, 1982, 1997). These fluctuations in the amplitude and phase are called amplitude scintillation and phase scintillation, respectively. When amplitude scintillation occurs, it can be hard to distinguish GNSS signals from noise due to reduction of signal-to-noise ratio. In contrast, the phase scintillation causes a phase shift exceeding the locked loop bandwidth in a worst case (Basu & Groves, 2001). The receiver then loses the signals, and time is wasted to recover the signal lock. Because the navigation services of the GNSS, including positioning and timing, are used anywhere, it is important to investigate the characteristics of ionospheric scintillations.

Ionospheric electron density irregularities related to scintillation at high latitudes have been investigated over the last few decades (Aarons, 1982; Basu et al., 1995, 1998; Clausen et al., 2016; Kelley et al., 1982; Prikryl et al., 2015; Spogli et al., 2009). From those studies, it is discovered that the phase scintillation frequently occurs at high latitudes near dayside polar cusp and nightside auroral region. The occurrences of the phase scintillation increase with solar activity and geomagnetic activity. At high latitudes, a two-cell convection pattern forms under a southward interplanetary magnetic field (IMF) (Knudsen et al., 1977). Following the convection, the ionospheric plasma moves antisunward in the noon sector in magnetic

©2020. The Authors.

This is an open access article under the terms of the Creative Commons Attribution-NonCommercial-NoDerivs License, which permits use and distribution in any medium, provided the original work is properly cited, the use is non-commercial and no modifications or adaptations are made.

local time (MLT). Large amounts of photoionized plasma flow from the midlatitude into the high-latitude region along the convection; this stream is called tongue of ionization (TOI) (Foster et al., 2005; Sojka et al., 1993). Occasionally, a high-density plume can detach from the TOI and form a polar cap patch (Carlson et al., 2004; Crowley et al., 2000; Zhang et al., 2013). Generally, the polar cap patch is defined as the region in which the ionospheric electron densities are at least 2 times greater than the background electron density. This means that the steep plasma density gradient in the polar cap patch exceeds the longitudinal and latitudinal density gradients that are naturally formed by solar radiation. Based on simulations, Sojka et al. (1998) showed that the growth rate of the gradient drift instability, which causes the ionospheric irregularity, is large around the polar cap patch. Therefore, the fast plasma flows (few kilometers per second) (Valladares et al., 1994) and accompanying steep plasma density gradients near the edge of the TOI or polar cap patch may cause large-scale (a few kilometers) ionospheric irregularities, which in turn induce phase scintillation at high latitudes (Basu et al., 1990). The effects of the polar cap patch on the electromagnetic signals have been studied in the very high frequency (Basu et al., 1990; Weber et al., 1986) and ultrahigh-frequency ranges (Jin et al., 2014; Van der Meer et al., 2014).

In addition to the fast flows of plasma along the convection, the energetic particle precipitation in the polar cap region (open magnetic flux tubes connected to the IMF) or auroral region (closed flux tubes of the plasma sheet) may be another cause of ionospheric electron density irregularities. The energetic particles from the magnetosphere can penetrate the altitudes of the *E* or *F* layers and partially ionize atmospheric neutral components in these regions (Voss & Smith, 1979). Resultant sporadic plasma density discontinuities near the aurora can create phase scintillation (Jin et al., 2015; Spogli et al., 2009). Wang et al. (2016) also reported that the main sources of the phase scintillation at high latitudes are fast flows of plasma and/or energetic particle precipitation. The polar cusp is the region in which solar wind plasma can directly enter the low altitudes from the magnetosheath and ionize thermospheric neutral components (Heikkila & Winningham, 1971). Particle precipitation in the polar cusp produces polar cap patches without the TOI or enhances preexisting patches. When additional ionization processes by cusp precipitation are sufficient to differentiate the higher-density region from the background, a polar cap patch is created (Smith et al., 2000; Walker et al., 1999). The polar cap patches produced by cusp precipitation also move antisunward along convection flows, similar to classical polar cap patches that detach from the TOI (Goodwin et al., 2015). Therefore, the polar cusp region is also related to ionospheric scintillation (Basu et al., 1994; Jin et al., 2017; Prikryl et al., 2010).

To determine typical scintillation characteristics, several climatological studies of ionospheric phase scintillation at high latitudes (Prikryl et al., 2015; Spogli et al., 2009) and model studies (Secan et al., 1997; Wernik et al., 2007) have been conducted. Li et al. (2010) reported that phase scintillation occurs more often in winter than in summer over Svalbard. Prikryl et al. (2015) showed that phase scintillations are more frequent during the solar maximum period and that the seasonal variation of phase scintillation maximizes in autumn and winter in the Northern Hemisphere. The high-latitude scintillation in the Southern Hemisphere was investigated during the geomagnetic storm period (Kinrade et al., 2012). The results showed that phase scintillation occurrences are associated with enhanced energetic particle precipitation in the dayside polar cusp region as well as an enhanced plasma density structure such as polar cap patch. Kinrade et al. (2013) statistically analyzed the association between GNSS scintillation and auroral emission. The correlation levels between optical auroral activities based on atomic oxygen emission peaked at 557.7 and 630.0 nm and the phase scintillation index reached up to 74% and 63%, respectively. However, that study was limited to auroral activities based on ground-based all-sky imager measurements; therefore, the overall characteristics of ionospheric scintillation in the Southern Hemisphere could not be determined. Thus, investigation of the ionospheric scintillation in the Southern Hemisphere is required.

To quantify the ionospheric scintillation, S_4 and σ_ϕ were defined as amplitude and phase scintillation indices, respectively (Briggs & Parkin, 1962; Yeh & Liu, 1982). The equations for these indices are as follows:

$$S_4 = \sqrt{\frac{\langle I^2 \rangle - \langle I \rangle^2}{\langle I \rangle^2}} \quad (1)$$

$$\sigma_\phi = \sqrt{\langle \phi^2 \rangle - \langle \phi \rangle^2} \quad (2)$$

where I is the signal strength, ϕ is the detrended carrier phase, and $\langle a \rangle$ represents the mean value of a data set a . It is known that the ionospheric scintillation index is related to the sizes of ionospheric irregularities (Forte & Radicella, 2002). Amplitude scintillation is caused by the irregularities smaller than the Fresnel radius (~ 300 m at L-band frequency) (Kintner et al., 2007). In contrast, phase scintillation is highly sensitive to large-scale (few kilometers) irregularities, causing refraction in signals (Forte, 2005). Since Fremouw et al. (1978) used the fixed cutoff frequency of 0.1 Hz for detrending wideband satellite data, it has been generally adopted to filter GNSS signals. However, the Fresnel frequency is expressed as function of the relative drift velocity of plasma (Forte, 2007; Forte & Radicella, 2002) such that 0.1 Hz corresponds to the relative drift velocity of ~ 30 m/s, which is significantly smaller than the typical plasma velocity at high latitudes of few hundreds of meters per second (Ruohoniemi et al., 1987; Tsunoda, 1988). Therefore, appropriate cutoff frequency corresponding to the plasma velocity is suggested, and there was an attempt to differentiate diffractive and refractive effects using a band-pass filter and obtained pure diffractive effects representing the ionospheric scintillation (McCaffrey & Jayachandran, 2019; Mushini et al., 2012). However, it is difficult to select the proper cutoff frequency, especially in statistical studies (De Franceschi et al., 2019). Although the detrending GNSS signal using 0.1 Hz may not be fully understood as phase scintillation, we used the typical 0.1 Hz as fixed cutoff frequency in this study to statistically investigate the characteristics of the ionospheric irregularities.

Multi-instruments-based studies including the provision of a scintillation map are helpful to determine the large-scale morphology of scintillation. However, single-point investigations are very similar to the environments of the users of GNSS-related services. A single-frequency system is applied to most of the commercial portable devices. This means that an ionosphere-free technique using dual-frequency cannot be used to remove the ionospheric effects from signals; therefore, the use of commercial devices is very sensitive to ionospheric conditions. In addition, it is not serviceable when strong scintillation accompanies the loss of signal lock. Therefore, user guidance must be established by characterizing the high-latitude ionospheric scintillation recorded at a single station. Here, we determined the characteristics of ionospheric scintillation indices using data measured at a high-latitude station in the Southern Hemisphere. Statistical analyses of ionospheric phenomena causing plasma density irregularities, such as the polar cap patch, polar cusp, and auroral oval, were conducted. We also statistically analyzed field-aligned currents (FACs) having the sizes of several kilometers and compared them with the scintillation results to determine which phenomenon is related to the climatological morphology of the scintillation.

2. Data and Methodology

The Korea Polar Research Institute (KOPRI) established Jang Bogo Station (JBS) in Antarctica (74.62°S , 164.22°E) in 2014. The geomagnetic latitude of JBS is 77.21°S . Therefore, JBS is suitable for investigations of the high-latitude ionosphere in the polar cap region. The Korea Astronomy and Space Science Institute (KASI) has been operating an ionospheric scintillation monitor, Connected Autonomous Space Environment Sensor (CASES), since December 2016. It can detect Global Positioning System (GPS) signals in both the L1 (1575.42 MHz) and L2 (1227.60 MHz) channels with high- and low-resolution modes. In low-resolution mode, the scintillation monitor records the carrier phase, pseudorange, and satellite position. When the user sets the parameters for the calculation of ionospheric scintillation indices (amplitude scintillation index: S_4 ; phase scintillation index: σ_{ϕ}), it routinely calculates the indices. In this study, we set the cutoff frequency to 0.1 Hz for the high-pass filtering of the signal intensity and phase. The time window was fixed to 100 s for the calculation of the scintillation indices. Raw information of GNSS signals, such as the carrier phase, in-phase accumulation (I), and quadrature accumulation (Q), was recorded at a high resolution of 100 Hz when the filtered signal power ratio reached a threshold. Figure 1 shows the locations of JBS (blue star) and south geomagnetic pole (red star). The blue and red circles represent the area corresponding to an elevation angle of 30° with respect to JBS at the altitude of 350 km and the geomagnetic latitude of 75°S at the same altitude, respectively. Note that the geomagnetic pole is located southwest of JBS.

In the present study, we utilized automatically computed scintillation indices to investigate the statistical characteristics of ionospheric scintillation at high latitudes. Although the scintillation indices used in this study have a low resolution (100 s), they can be used to explore the statistical behavior. Scintillation indices with high resolution (e.g., 1 s) can be achieved using high-resolution measurements of raw signal

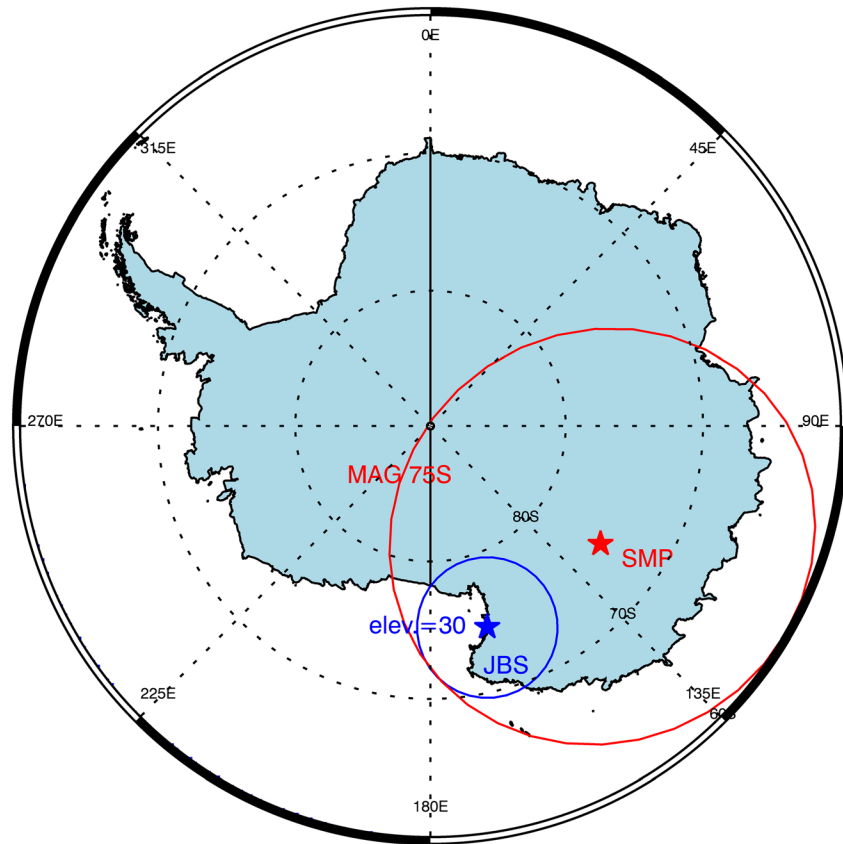


Figure 1. Locations of the Jang Bogo Station (JBS) and south geomagnetic pole. The blue circle indicates the sector with an elevation angle of 30° with respect to JBS at an altitude of 350 km. The red circle represents the geomagnetic latitude of 75°S at the same altitude.

information (100 Hz) and can be used to more sensitively detect scintillation events. However, the high-resolution data set for the statistical study is considerably dense; therefore, the analysis is time-consuming. The total number of the scintillation indices based on the low-resolution data for both amplitude and phase is 9,463,055 for the 2-year period (2017–2018); it is sufficient for a statistical study. The scintillation indices measured by CASES were binned with an elevation angle of 10° and azimuth angle of 15° to obtain the distribution of the scintillation occurrence rates. The occurrence rate of the ionospheric scintillation in each bin was computed as follows:

$$\text{occurrence rate [\%]} = \frac{\text{number of scintillation index} \geq 0.2}{\text{total number of scintillation index}} \times 10 \quad (3)$$

We set both S_4 and σ_ϕ to 0.2 to detect all scintillation events including weak ones. The occurrence rates of the scintillation in each bin were calculated for different groups following parameters: MLT, seasons, geomagnetic activity, and signal type. Details of the distributions are listed in Table 1.

Table 1 <i>Parameters and Their Criteria for Grouping the Ionospheric Scintillation Cases Over the Jang Bogo Station (JBS)</i>	
Parameters	Criteria
Magnetic local time (MLT) (hour)	21–03 (midnight)/03–09 (dawn)/09–15 (noon)/15–21 (dusk)
Season	March Equinox (February–April)/June Solstice (May–July)/September Equinox (August–October)/December Solstice (November–January)
Geomagnetic activity	High K_p (>2)/low K_p (≤2)
Signal type	L1 (1575.42 MHz)/L2 (1227.60 MHz)

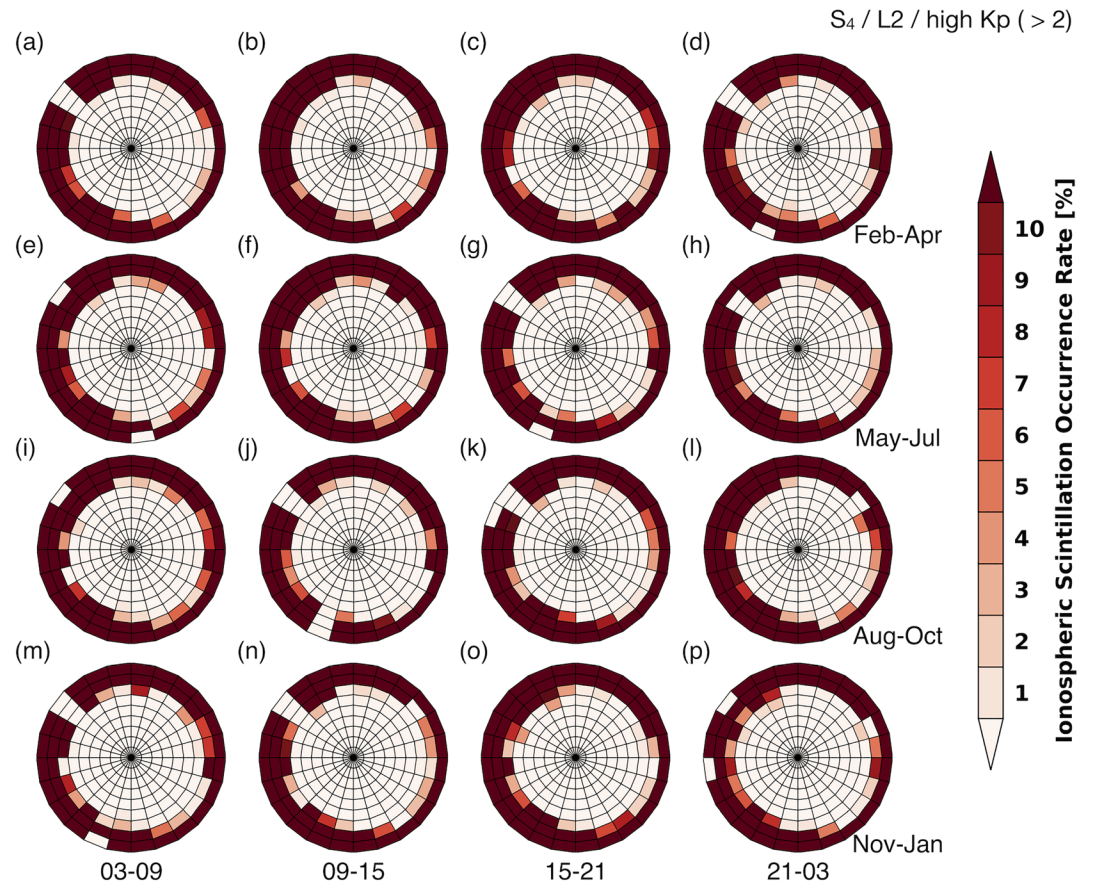


Figure 2. (a–p) Occurrence rates of the amplitude scintillation index (S_4) in the GPS L2 channel over the Jang Bogo Station (JBS) during 2 years (2017–2018) under geomagnetically disturbed conditions. The upward direction indicates geographic north and the center of the plot is the zenith of JBS. From left to right, each column shows the dawn, noon, dusk, and midnight sectors based on magnetic local time, respectively. From top to bottom, each row displays the March equinox, June solstice, September Equinox, and December solstice, respectively.

Magnetized solar wind, including charged particles, encounters the magnetosphere and the IMF is reconnected with the Earth's magnetic field. The induced dawn-to-dusk electric field and the perpendicular magnetic field line at high latitude cause the antisunward movement of plasma. Hence, it is more appropriate to divide the data with respect to the MLT rather than universal time (UT) or solar local time (LT) based on the electrodynamic coupling at high latitude. The MLT sectors are centered at 0 (midnight), 6 (dawn), 12 (noon), and 18 (dusk). To explore the seasonal effects and geomagnetic dependencies, the data set was divided based on seasons (equinoxes and solstices) and the K_p index (>2 and ≤ 2). All processes were equally applied to both the L1 and L2 channels to determine signal frequency dependencies.

3. Results

3.1. Occurrence Rates of the Amplitude Scintillation Index

Figure 2 shows the occurrence rates of amplitude scintillation index (S_4) in the GPS L2 channel during high geomagnetic activity ($K_p > 2$). The outermost bins of each plot indicate the lowest elevation angle ($0\text{--}10^\circ$) with respect to JBS and the elevation angle increases by 10° toward the center of the plot (zenith of JBS). The upward direction toward the top of the page represents the geographic north and the azimuth angle increases in the clockwise direction. White and red colors represent lower and higher occurrence rates of amplitude scintillation, respectively. In Figure 2, each row from the top to bottom represents the March equinox (local fall), June solstice (local winter), September equinox (local spring), and December solstice (local summer), respectively. Each column from the left to right represents the MLT dawn, noon, dusk,

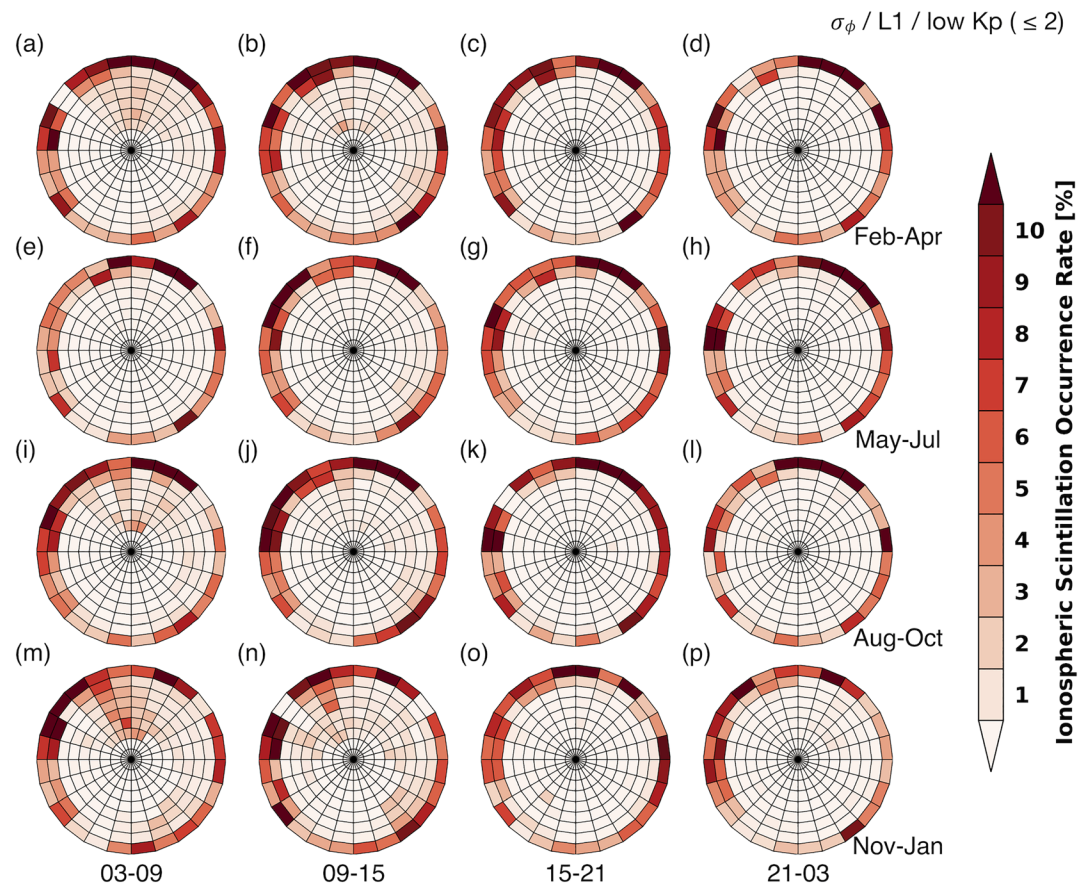


Figure 3. (a–p) Occurrence rates of the phase scintillation index (σ_ϕ) in the GPS L1 channel over the Jang Bogo Station (JBS) during 2 years (2017–2018) under geomagnetically quiet conditions. The upward direction indicates geographic north, and the center of the plot is the zenith of JBS. From left to right, each column shows the dawn, noon, dusk, and midnight sectors based on magnetic local time, respectively. From top to bottom, each row displays the March equinox, June solstice, September Equinox and December solstice, respectively.

and midnight sector, respectively. The figure shows that the occurrence rates of amplitude scintillation can be divided into two parts by the elevation angle of 30° . Amplitude scintillation occurs very frequently at lower elevation angles below 30° irrespective of the MLT, season, and azimuth angle. However, amplitude scintillation is almost absent (lower than 1%) at higher-elevation angles above 30° . Similar distributions are obtained for the GPS L1 channel and geomagnetically quiet conditions (not shown).

3.2. Occurrence Rates of the Phase Scintillation Index

Figure 3 is the same as Figure 2 but for the occurrence rates of phase scintillation (σ_ϕ) of the GPS L1 channel under the geomagnetically quiet conditions. The phase scintillation also has higher occurrence rates at lower elevation angles, similar to the amplitude scintillation, but not as extreme. The high occurrence rates of phase scintillation are concentrated at slightly lower elevation angles ($10\text{--}20^\circ$) than those of amplitude scintillation (30°). In these cases, only a few bins exceed 10%, and mostly higher occurrence rates ($\geq 10\%$) are observed for amplitude scintillation. In contrast to the amplitude scintillation occurrence rates, the occurrence rates of phase scintillation above 30° show significant values with distinct seasonal/MLT dependencies. First, the occurrence rates are maximal during the December solstice and minimal during the June solstice. Second, the occurrence rates in the MLT dawn and noon sectors are higher than those in the MLT dusk and midnight sectors. Third, phase scintillation frequently occurs in the geographically northeastern parts with respect to JBS. Figure 4 is the same as Figure 3 but for the GPS L2 channel; the occurrence rate distributions are very similar to those of L1.

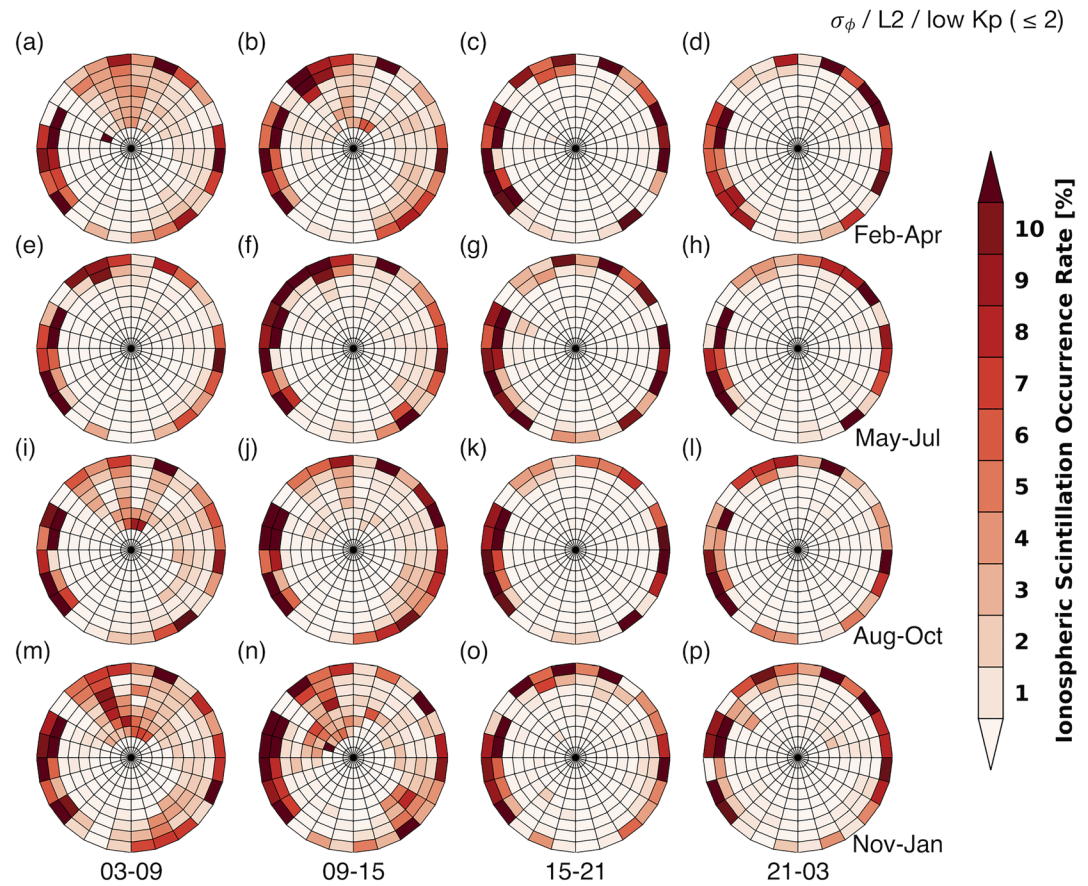


Figure 4. (a–p) Occurrence rates of the phase scintillation index (σ_{ϕ}) in the GPS L2 channel over the Jang Bogo Station (JBS) during 2 years (2017–2018) under geomagnetically quiet conditions.

Figures 5 and 6 are the same as Figures 3 and 4 but for geomagnetically disturbed conditions. The comparison of Figures 3–6 shows that the occurrence rates are not only higher in the GPS L2 channel than in the L1 channel, but they are also higher under disturbed geomagnetic conditions than under quiet conditions. As an extreme example, in the GPS L2 channel under disturbed geomagnetic conditions in the MLT noon sector in December (Figure 6), the phase scintillation occurrence rates exceed 10%, even in the vicinity of the zenith where the GNSS signal passes through the ionosphere via the shortest path. Furthermore, from Figures 3–6, the scintillation occurrence rate variations depending on the MLT, season, and azimuth angle are increasingly recognizable. Although the occurrence rates are dramatically enhanced in the GPS L2 channel under disturbed geomagnetic conditions (Figure 6), the occurrence rates almost remain constant at low magnitudes in the MLT dusk, midnight sectors, and during the June solstices (Figures 6g and 6h). The occurrence rates southwest of JBS also remain low in all seasons and MLT sectors (Figure 6).

3.3. Effects of the Elevation Cutoff

Generally, a cutoff elevation angle of 15–20° is used in ionospheric research. In this study, all occurrence rates of amplitude scintillation below 20°, and several bins at the elevation angles of 20–30° show very high magnitudes. This implies that slant GPS signals with low-elevation angles can be contaminated by multipath effects such that it is not appropriate to consider them as ionospheric irregularity effects. It is a matter of course that the GPS signals might be affected by the ionospheric irregularities. However, it is difficult to distinguish two effects at low-elevation angle. Hence, we only considered the region with an elevation angle above 30° to determine correlations with ionospheric irregularities. Figure 7 presents the averaged phase scintillation occurrence rates at elevation angles above 30° as a function of the azimuth angle. Different colors indicate different seasons. From top to bottom, each row represents the MLT dawn, noon, dusk, and

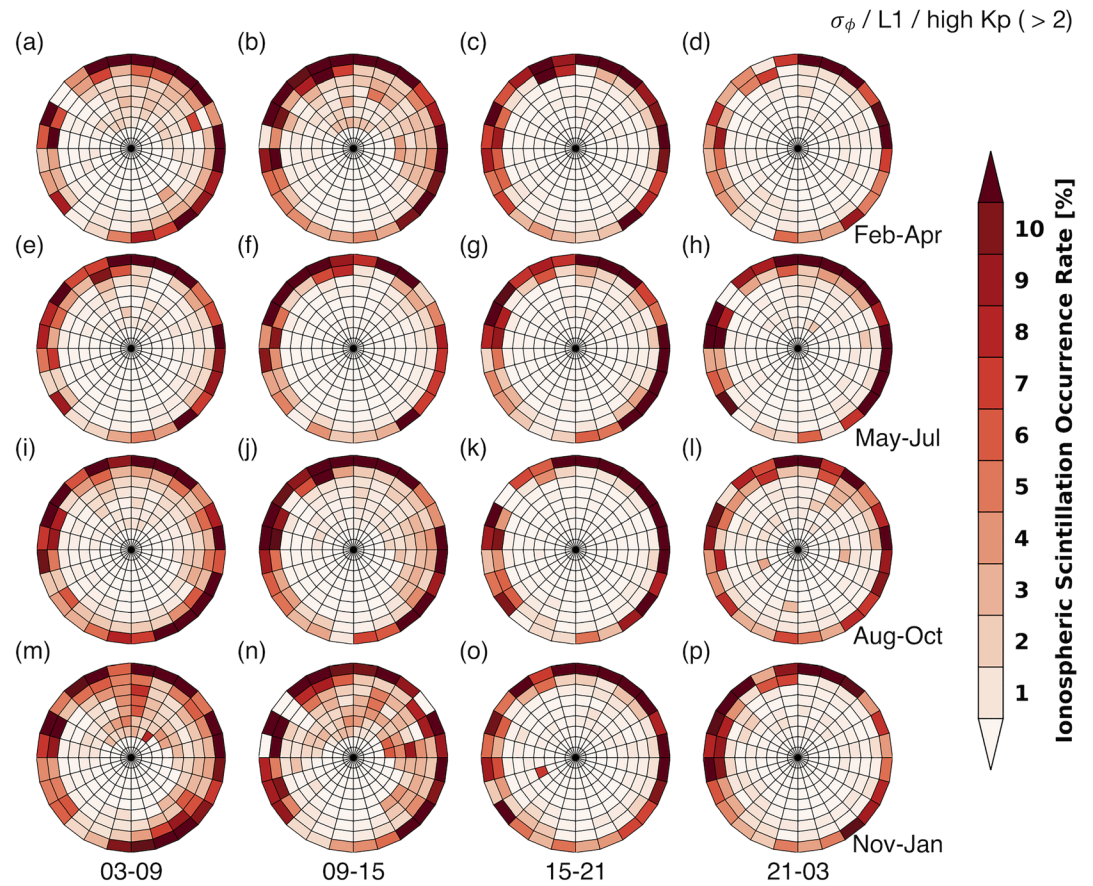


Figure 5. (a–p) Occurrence rates of the phase scintillation index (σ_{ϕ}) in the GPS L1 channel over the Jang Bogo Station (JBS) during 2 years (2017–2018) under geomagnetically disturbed conditions.

midnight sectors, respectively. Red arrows represent the direction of the south geomagnetic pole with respect to JBS. The vacancies around the azimuth angle of 180° are due to the observation limit imposed by the GPS satellite inclination. The figure shows that the phase scintillation occurrence rates are higher in the MLT dawn and noon sectors, but almost 0 in the MLT dusk and midnight sectors. During May–July (green lines), the occurrence rates are extremely low in all MLT sectors. The occurrence rates increase into the northern and eastern directions from the JBS. In contrast, the occurrence rates decrease toward the south geomagnetic pole ($\sim 223^{\circ}$). The occurrence rates are $\sim 1\%$ in the northern and eastern directions, except for the June solstice (Figures 7a and 7b). The strongest occurrence rates during the December solstice reach up to $\sim 4\%$ in the MLT dawn sector (Figure 7a).

Figure 8 is the same as Figure 7 but for the GPS L2 channel. The occurrence rates of the L2 channel under geomagnetically quiet conditions slightly increase by $\sim 1\%$ in the northeastern direction ($0\text{--}45^{\circ}$) in the MLT dawn and noon sectors compared with the L1 channel. The maximum occurrence rates exceed 5% during the December solstice in the MLT dawn and noon sectors, except for outliers (Figures 8a and 8b). However, the occurrence rates in the MLT dusk and midnight sectors are very low (Figures 8c and 8d). Figures 9 and 10 are the same as Figures 7 and 8, respectively, but for geomagnetically disturbed conditions. Phase scintillation more frequently occurs under geomagnetic disturbances. Although the maximum value of $\sim 4\%$ is similar to the value under quiet geomagnetic conditions, the occurrence rates of the L1 channel in the MLT dawn and noon sectors increase by $\sim 1\text{--}3\%$ at all elevation angles, except for the geomagnetic pole direction (Figures 9a and 9b). The L2 channel shows very high occurrence rates under geomagnetic disturbances compared with other cases. Although we set vertical axis range to 0–5% to easily compare different cases, the maximum occurrence rate reaches 12.6% in the MLT noon sector during the December solstice (Figure 10b). The occurrence rates during the equinoxes also increase and sometimes exceed 5%. Despite

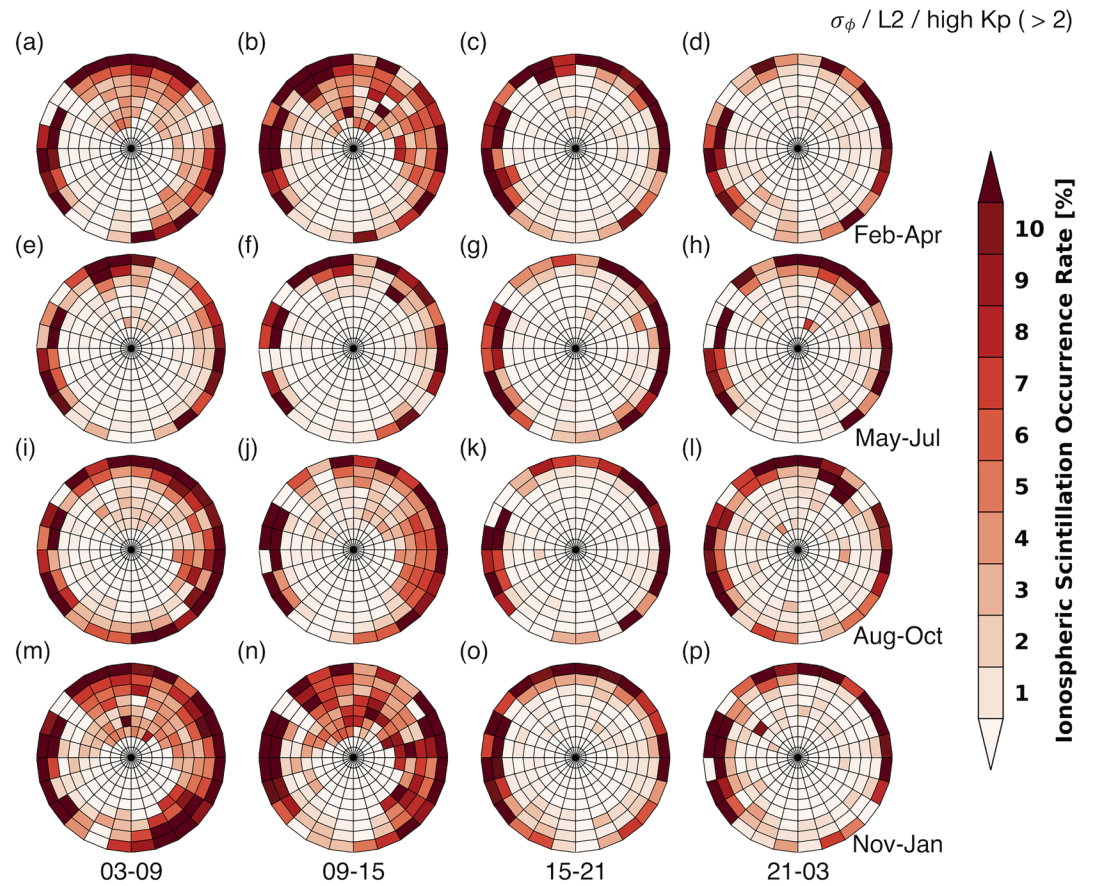


Figure 6. (a–p) Occurrence rates of the phase scintillation index (σ_{ϕ}) in the GPS L2 channel over the Jang Bogo Station (JBS) during 2 years (2017–2018) under geomagnetically disturbed conditions.

the increase in the scintillation occurrence rate, the MLT dusk and midnight sectors still show negligible phase scintillations, similar to geomagnetically quiet conditions (Figures 10c and 10d).

3.4. Statistical Characteristics of Ionospheric Phenomena Related to Scintillation

As mentioned in section 1, ionospheric scintillation is caused by ionospheric irregularities. Therefore, the statistical characteristics of the ionospheric scintillation should be strongly related to various ionospheric phenomena. In this part, we determined the sources of the ionospheric scintillation characteristics based on the statistical analysis of various irregularities. The Swarm mission by the European Space Agency (ESA) was launched in 2013 (Friis-Christensen et al., 2008). One pair of satellites (A and C) has an altitude of ~ 456 km and another satellite (B) has a higher altitude of ~ 530 km. These satellites conduct in situ measurements of the magnetic field as well as the electron density along their trajectories. Ionospheric electron densities measured at the altitudes of Swarm satellites with 0.5-s time resolution are used to detect the polar cap patches. Magnetic field measurements with 50-Hz time resolution in the instrument (Vector Field Magnetometer) frame after rotation into the spacecraft coordinate system by a matrix are used to estimate small-scale FACs. The Defense Meteorological Satellite Program (DMSP) mission by the National Oceanic and Atmospheric Administration (NOAA) has been operated to monitor not only meteorological and oceanographic phenomena but also solar-terrestrial physics since the 1960s (Nichols, 1976). Energetic particle precipitation measurements by the Precipitation Electron/Proton Spectrometer SSJ/5 on board the DMSP are used to estimate the polar cusp location and time.

3.4.1. Polar Cap Patch Effect

As mentioned in section 1, the polar cap patch is one of the major sources of ionospheric irregularities at high latitudes. Hence, we statistically analyzed the polar cap patch occurrences over JBS during the study

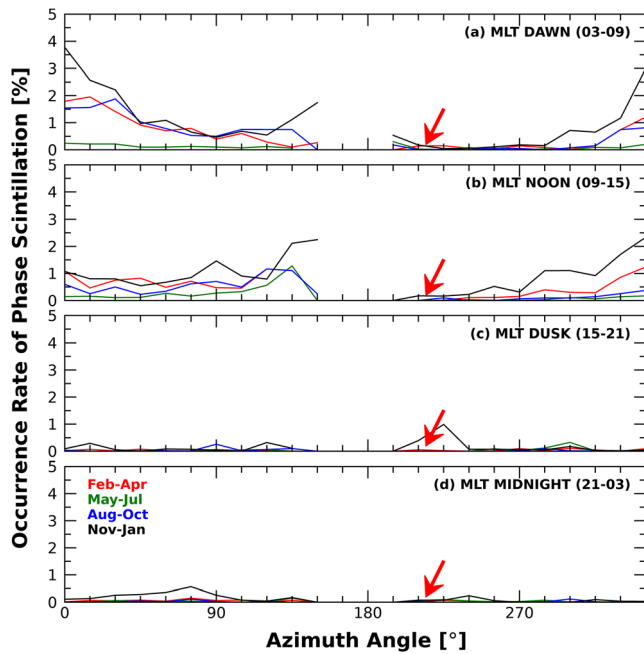


Figure 7. (a–d) Averaged occurrence rates of the phase scintillation index (σ_{ϕ}) at elevation angles above 30° versus the azimuth angle in the GPS L1 channel over the Jang Bogo Station (JBS) during 2 years (2017–2018) under geomagnetically quiet conditions. The red arrows indicate the direction of the south geomagnetic pole with respect to JBS. The four different colors represent the different seasons. From top to bottom, each row shows the dawn, noon, dusk, and midnight sectors based on magnetic local time.

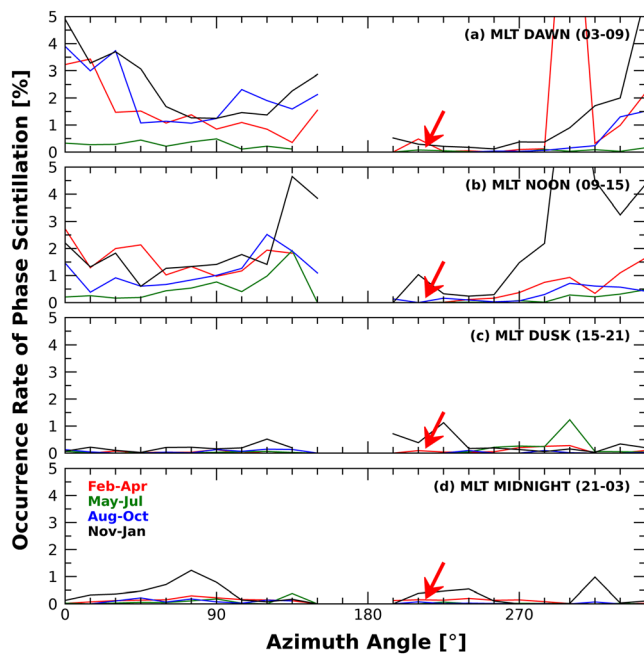


Figure 8. (a–d) Averaged occurrence rates of the phase scintillation index (σ_{ϕ}) at elevation angles above 30° versus the azimuth angle in the GPS L2 channel over the Jang Bogo Station (JBS) during 2 years (2017–2018) under geomagnetically quiet conditions.

period. Noja et al. (2013) counted polar cap patches using up-looking total electron contents (TECs) data produced by the Challenging Minisatellite Payload (CHAMP) satellite. They reported a higher number of polar cap patches during the December solstice and equinoxes in both hemispheres. On the other hand, Spicher et al. (2017) used in situ plasma density measured by Swarm satellites and reported frequent polar cap patches in the winter hemisphere. Chartier et al. (2018) proved that the inconsistency between the two studies regarding the polar cap patch occurrence originates from the different methodologies; both techniques have defects, the erroneous detection of polar cap patches. They suggested a better algorithm to more precisely detect the polar cap patches. By applying the algorithm suggested by Chartier et al. (2018) to in situ electron density data measured by the Swarm Satellites A, B, and C, we counted the polar cap patches over JBS. The three major contents detecting the polar cap patches introduced by Chartier et al. (2018) are follows: (1) in situ measurements of ionospheric electron density applying smoothing filter must show a 40% increase within 140 km and a 40% decrease within following 140 km, (2) the highest density within the patch must be greater than double the background density, and (3) the patch peak is defined to be greater than 1,500-km mean by 1,000 times the 81-day-averaged $F_{10.7}$ solar flux index. The total number of polar cap patches in the Southern Hemisphere in the period of 2017–2018 is 10,345. The number of polar cap patches over JBS, which was determined by filtering the polar cap patches within 800 km from the zenith of JBS at Swarm satellites altitudes (A and C ~456 km; B ~530 km), is 807. Figures 11a and 11b show the number distributions of polar cap patches over JBS as a function of the MLT and day of the year (DOY), respectively. The four different colors in Figure 11b indicate the four seasons. Figure 11a shows that the polar cap patches occur most frequently in the MLT noon sector and least frequently in the MLT dawn and dusk sectors. This implies that the polar cap patches mainly form on the dayside and then move, following the convection pattern of plasma at high latitudes. The MLT variations of the polar cap patches match our results for the phase scintillation MLT variation over JBS (Figures 7–10). Figure 11b shows the clear seasonal variations of the polar cap patches over JBS. Polar cap patches barely occur during the June solstices (green), whereas they are maximal during the December solstices (black), which is very similar to the seasonal variation of the phase scintillation over JBS (Figures 7–10). Noja et al. (2013) suggested that the mechanism that enhances the TECs during the December solstice due to the global ionospheric seasonal asymmetry may increase the potential to transport the higher plasma densities to the polar cap region, which would lead to the more frequent formation of polar cap patches during the December solstice. Hence, we infer that the higher occurrence of polar cap patches during the December solstice may induce the higher occurrence of the phase scintillation during the December solstice.

3.4.2. Polar Cusp Effect

To compare the seasonal and local time variations of the phase scintillation with that of the polar cusp, we determined the polar cusp locations by analyzing data from the Precipitation Electron/Proton Spectrometer (SSJ/5) on board the DMSP satellites. Newell and Meng (1988) suggested criteria for estimating the polar cusp location from SSJ/5 data (i.e., energy flux of electrons, energy flux of ions, mean energy of electron, and mean energy of ion). By using the same method, we estimated the polar cusp

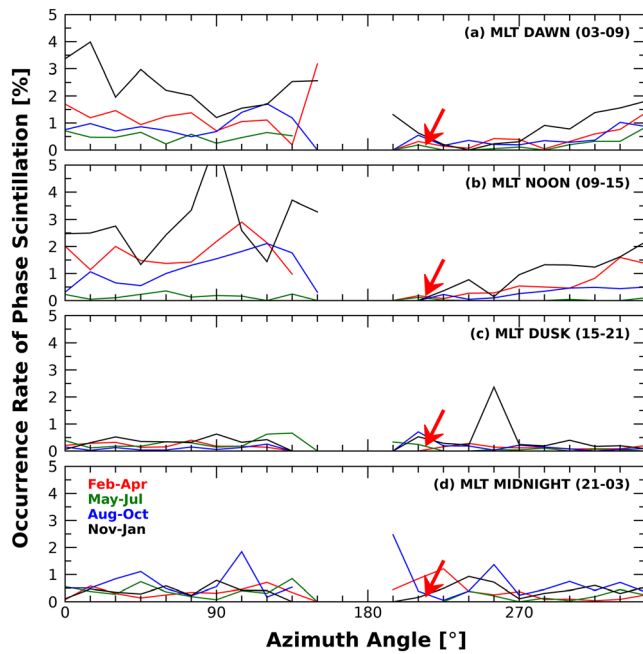


Figure 9. (a–d) Averaged occurrence rates of the phase scintillation index (σ_{ϕ}) at elevation angles above 30° versus the azimuth angle in the GPS L1 channel over the Jang Bogo Station (JBS) during 2 years (2017–2018) under geomagnetically disturbed conditions.

tion to determine the azimuth angle dependency and MLT dawn-dusk asymmetry. Xiong et al. (2014) statistically investigated the auroral oval location using CHAMP magnetic field data during a solar cycle. They estimated the equatorward and poleward boundaries of the auroral oval for various geomagnetic activities

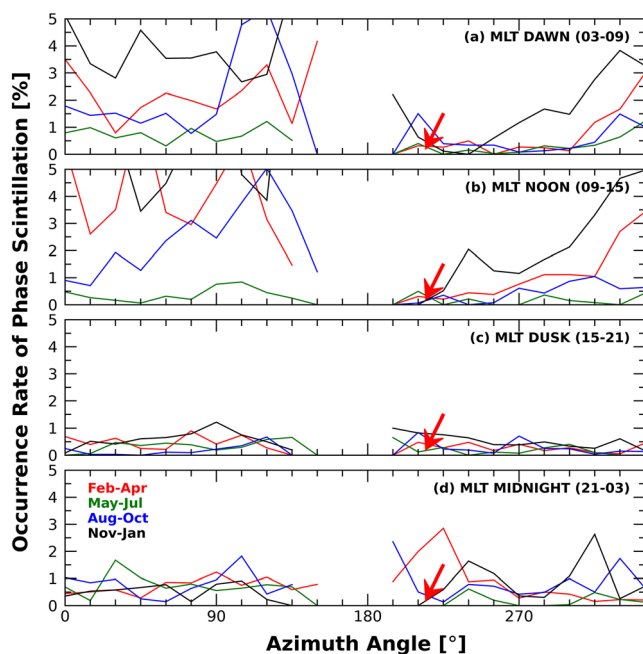


Figure 10. (a–d) Averaged occurrence rates of the phase scintillation index (σ_{ϕ}) at elevation angles above 30° versus the azimuth angle in the GPS L2 channel over the Jang Bogo Station (JBS) during 2 years (2017–2018) under geomagnetically disturbed conditions.

location and MLT using DMSP f16, f17, and f18 satellites during the study period (2017–2018). The total number of the estimated points for the polar cusp is 48,906. Table 2 presents the average polar cusp locations and MLTs for four seasons. The polar cusp mainly forms in the MLT prenoon sector (10–11 MLT) in all seasons. The polar cusp is located at geomagnetic latitudes of 73° – 74° S. In Figure 1, the circle of the elevation angle of 30° from JBS is tangent to the circle of the geomagnetic latitude of 75° S at opposite direction toward southern geomagnetic pole. Therefore, the polar cusp is generally located at northeast of JBS. The location of the polar cusp slightly changes depending on the season; it is at the highest geomagnetic latitude during the December solstice. Thus, the polar cusp analysis has two similarities to the phase scintillation analysis, that is, higher occurrence rates of the phase scintillation in the (1) MLT noon sector during the (2) December solstice. The higher occurrence rates of the phase scintillation in the MLT noon sector (09–15 MLT) match the MLT of the generated polar cusp. This indicates that the polar cusp near the MLT noon contributes to ionospheric phase scintillation events through the additional ionization processes based on cusp precipitation. Although the seasonal variation of the polar cusp location is very small, it is reasonable to presume that the proximity of the polar cusp to JBS during the December solstice may play a part in the frequent occurrence of phase scintillation in this period compared with other seasons.

3.4.3. Poleward Auroral Oval Effect

Although the JBS is located in the polar cap region, we need to consider the relationship between the phase scintillation and the auroral oval location to determine the azimuth angle dependency and MLT dawn-dusk asymmetry. Xiong et al. (2014) statistically investigated the auroral oval location using CHAMP magnetic field data during a solar cycle. They estimated the equatorward and poleward boundaries of the auroral oval for various geomagnetic activities and then derived the ellipse parameters of the auroral oval boundaries. We reproduced the auroral oval in the Southern Hemisphere using the ellipse parameters of Xiong et al. (2014). Figure 12 presents the auroral oval reproduced for the Southern Hemisphere under three different geomagnetic conditions. Gray shades indicate the modeled auroral ovals. The blue dotted lines represent the geomagnetic altitude of 75° S, which is close to the limit for meaningful measurements for ionospheric study using GNSS, as previously mentioned in Figure 1. The areas marked with a light shade denote the meaningful observation limits overlapping with the auroral oval. The marked area is wider in the MLT dawn sector than in the MLT dusk sector, implying that the dawn sector is more affected by auroral activities and thus more prone to phase scintillation. Furthermore, Drury et al. (2003) noted that poleward-moving auroral forms (PMAFs) in the Southern Hemisphere have morning bias. Oksavik et al. (2015) also reported that PMAFs caused strong plasma irregularities with scales ranging from a few hundred meters to a few kilometers and severe phase scintillation events. Furthermore, Van der Meeren et al. (2015) reported severe phase scintillation at the poleward edge of the auroral oval during an intense substorm aurora. This means that more active auroral activities, including PMAFs in the MLT dawn sector, may be the sources of the higher phase scintillation occurrences in the MLT dawn sector detected by ground-based observations. Furthermore, the auroral oval is located in the sector northeast of JBS (away from the pole), which may cause higher scintillation occurrence rates northeast of JBS compared with the part southwest of JBS (close to the pole).

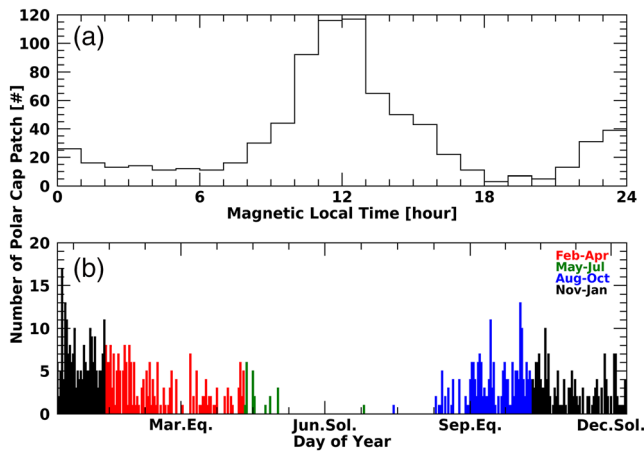


Figure 11. Number of polar cap patches over Jang Bogo Station (JBS) estimated from Swarm satellites versus the (a) magnetic local time and (b) day of year, respectively. The four different colors indicate the different seasons.

3.4.4. Effects of FACs

Although we find more poleward expanded auroral oval in the MLT dawn sector may be related to the higher occurrence rates of phase scintillation, it is not sufficient to create the dramatic asymmetry of the phase scintillation occurrence rates between the MLT dawn and dusk sectors. Hence, we further investigated the FACs. Park et al. (2012) showed that medium-scale FACs (based on 1-Hz magnetic field data) are collocated with ionospheric irregularities, which may lead to stronger ionospheric scintillations in the prenoon sector than in the postnoon sector. Large-scale FAC structures are unlikely to induce ionospheric scintillation, whereas small- or medium-scale FAC structures can generate irregularities that cause scintillation. Each Swarm satellite measures the magnetic field at high-resolution (50 Hz). Ritter et al. (2013) introduced the calculation of FACs from in situ measurements of the magnetic field. The ESA provides Level-2 processed FACs data with low resolution (1 Hz) from Swarm observations (Ritter et al., 2013). However, we focused on small-scale structure below 1 Hz in this study; therefore, we used Swarm Level-1 high-resolution magnetic field data with a 50-Hz time resolution. Because of the huge amount of high-resolution data, we only

chose 20 days close to the equinoxes and solstices for the Swarm Satellites A, B, and C. Only components of magnetic field data between 1 and 25 Hz (corresponding to a spatial resolution of ~ 7.5 and ~ 0.3 km, respectively) were filtered. The FACs were then derived by using a method similar to that reported in Ritter et al. (2013). Subsequently, only the FAC data points within 800 km from the zenith of JBS were selected as the FACs over JBS, similar to the methodology used to detect the polar cap patches.

Figure 13 displays the mean absolute deviations (MADs) of the small-scale FAC amplitudes as a function of the MLT for four seasons. The amplitudes of small-scale FACs show seasonal dependencies, with minima during the June solstice (green). The MLT variations intensify in the MLT dawn (03–09) sector compared with the MLT dusk (15–21) sector. The averaged amplitudes of the MADs in the MLT dawn and dusk sectors are presented in Table 3. The average amplitudes in the MLT dawn sector are almost 2 to 3 times those of the MLT dusk sector. Notable asymmetries of the small-scale FAC structures may lead to more frequent phase scintillation in the MLT dawn sector as well as during the December solstice. However, the exact causes for the FAC asymmetries in the MLT dawn and dusk sectors remain unclear and will be addressed in future studies.

4. Discussion

In this study, we investigated statistical morphologies of the amplitude and phase scintillations at high latitudes. The 0.1 Hz of cutoff frequency is used to automatically calculate the scintillation indices. Although it has been proposed that variable cutoff frequencies should be applied to removing refractive effects in case of deriving the scintillation indices at high latitudes (McCaffrey & Jayachandran, 2019; Mushini et al., 2012), it

is very hard to be used in our statistical study. As described in the introduction section, choosing an appropriate cutoff frequency for all cases is difficult without information regarding the plasma velocity or size of the irregularity. Recently, De Franceschi et al. (2019) used four different cutoff frequencies (0.1, 0.25, 0.4, and 1.0 Hz) to statistically investigate the phase scintillation in the Northern Hemisphere. The phase scintillation characteristics obtained by using different cutoff frequencies have a notable mismatch. The statistical analysis of the phase scintillation index, σ_ϕ , using 0.25- and 0.4-Hz cutoff frequencies was similar to the amplitude scintillation index, S_4 . The results obtained for the 0.1 Hz case were very similar to those of our study. Therefore, it should be noted that the results in our study might change if different cutoff frequencies were adopted. De Franceschi et al. (2019) used a cutoff frequency of 0.1 Hz to determine the statistical characteristics of large-scale ionospheric irregularities. Note

Table 2
Average Locations and Magnetic Local Times (MLTs) of the Polar Cusp Estimated From Data Obtained With the Precipitation Electron/Proton Spectrometer (SSJ/5) On Board the Defense Meteorological Satellite Program (DMSP) Satellites in the Southern Hemisphere During 2017–2018

	March equinox	June solstice	September equinox	December solstice
Location (geomagnetic latitudes)	73.98°S	73.49°S	73.36°S	74.14°S
Time (magnetic local time, MLT)	10.96 MLT	11.64 MLT	11.02 MLT	10.37 MLT

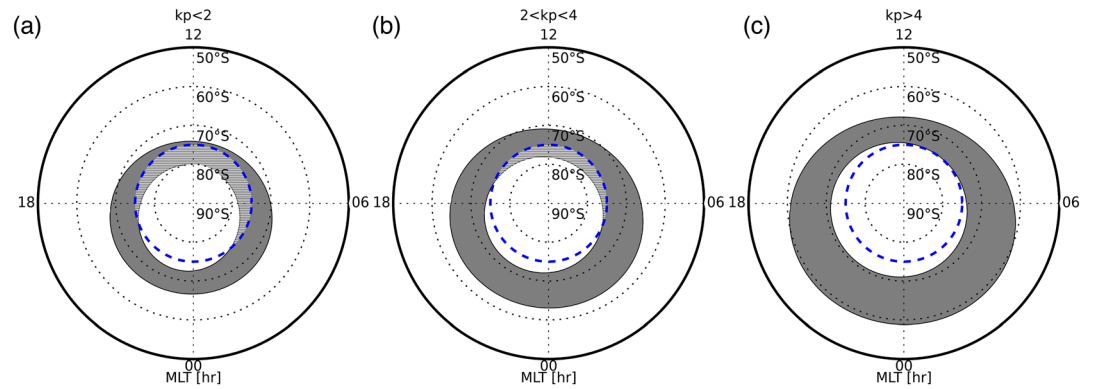


Figure 12. (a–c) Auroral oval (gray shades) reproduced for the Southern Hemisphere using ellipse parameters reported by Xiong et al. (2014). The blue dotted lines indicate the geomagnetic latitude of 75°S, which corresponds to observation limit over Jang Bogo Station (JBS). The areas with oblique lines represent regions in which the auroral oval overlaps with the observation limit. Each panel represents different geomagnetic conditions.

that Spicher et al. (2020; section 2) also adopted the conventional cutoff frequency of 0.1 Hz and justified their choice in detail. Therefore, the scintillation indices using 0.1 Hz of cutoff frequency are still valuable to explore the characteristics of the ionospheric scintillation at high latitudes. Although the phase scintillation occurrences in our study may partially originate from refractive effects (or both diffractive and refractive effects), the statistical approach to determine the characteristics of GNSS signal scintillation indices at high latitudes (especially Antarctica) provides insights into ionospheric irregularities.

The statistical characteristics of amplitude scintillation are simple; the high occurrence rates at elevation angles below 30° can be continuously observed throughout the entire season and time. As the elevation angle decreases, the ionospheric path of the GNSS signals from the satellites to the receivers increases, and thus, the distance passing through the irregular medium also increases. Briggs and Parkin (1962) reported the exponential increase of the relative scintillation depth for radio signals of stars and satellites at lower elevation angles. The amplitude scintillation index is expressed as a function of the cosecant of the elevation angle and the geometry propagation factor, which is given by the function of the elevation angle, as shown in Equations 31 and 34 in Rino (1979). Therefore, it has a complex relationship with the elevation angle. Although the irregular medium is not enough to cause the amplitude scintillation over 0.2 at higher-elevation angle, the amplitude scintillation index can be amplified at lower elevation angle. Priyadarshi and Wernik (2013) analyzed GPS scintillations based on the elevation angle. They compared them with the simulation results, confirming their strong dependence on the elevation angle; that is, the amplitude scintillation index exponentially intensifies with decreasing elevation angle. In addition, the multipath of the GNSS signals could also enhance the scintillation at low-elevation angles. The multipath effect, that is, the mixture of the GNSS signals from the ground or nearby objects with direct GNSS signals, causes

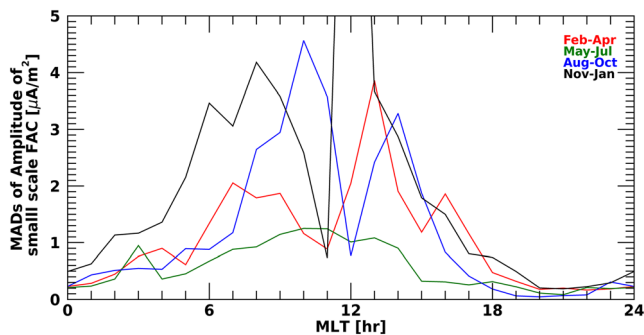


Figure 13. Amplitudes of small-scale field-aligned currents (FACs) over Jang Bogo Station (JBS) derived from Swarm satellites with a 1-Hz cutoff frequency.

errors in the measurements of the pseudorange or carrier phase (Kaplan & Hegarty, 2006). Hence, the observed high occurrence rates of amplitude scintillation at low-elevation angles, as shown in Figure 2, might originate from ionospheric irregularities or contamination from ambient noise such as the multipath effects. However, it is very difficult to determine the source of the high scintillation index at an elevation angle below 30°. On the other hand, no distinct amplitude scintillation at elevation angles above 30° in Figure 2 matches the results of previous studies (Jiao et al., 2013), which indicated infrequent amplitude scintillation at high latitudes.

In contrast to amplitude scintillation, the occurrence rates of the phase scintillation index show various characteristics. As we mentioned in the previous paragraph, the phase scintillation using a fixed cutoff frequency may be contaminated by refractive effects, but it still strongly correlates with the large-scale density irregularities. Statistical comparisons with

Table 3
Averaged Mean Absolute Deviations (MADs) of Small-Scale FAC Amplitudes (Below a Spatial Resolution of 7.5 km) Over JBS in the MLT Dawn (03–09) and in Dusk (15–21) Sectors Derived From High-Resolution Swarm Satellites Measurements

	MLT dawn	MLT dusk
March Equinox (February–April)	1.33 $\mu\text{A}/\text{m}^2$	0.77 $\mu\text{A}/\text{m}^2$
June Solstice (May–July)	0.77 $\mu\text{A}/\text{m}^2$	0.23 $\mu\text{A}/\text{m}^2$
September Equinox (August–October)	1.37 $\mu\text{A}/\text{m}^2$	0.50 $\mu\text{A}/\text{m}^2$
December Solstice (November–January)	2.71 $\mu\text{A}/\text{m}^2$	0.82 $\mu\text{A}/\text{m}^2$

ionospheric phenomena show notable similarities of seasonal and local time variations. The polar cap patch causing a steep plasma density gradient commonly occurs during the December solstice and in the MLT noon sector. It matches the maximum occurrence rates of the phase scintillation during this season and time. In addition, the polar cusp region in which energetic particles mainly precipitate into the ionosphere and partially ionize the neutrals causes the MLT noon dominance of the phase scintillation. Although a seasonal change of the polar cusp location is not noticeable, the polar cusp is mostly close to the JBS during the December solstice, maximizing the phase scintillation occurrence rates.

Auroral activity is considered to be another source of phase scintillation

despite the location of JBS. The poleward edge of the auroral oval expands toward high latitudes in the MLT dawn sector, more than in the MLT dusk sector. Based on the reproduction of a previous study (Xiong et al., 2014), we confirm that the overlap of the GNSS observation area with the auroral oval is large in the MLT dawn sector. Although the polar cap patch, polar cusp, and auroral activity are well-known sources of ionospheric irregularity, we suggest a potential relationship between small-scale FACs and the ionospheric irregularity in this study. Energetic electrons (ions) can penetrate the ionosphere along upward (downward) FACs. Therefore, the horizontal changes of the FAC direction at high latitudes may lead to periodic precipitation of energetic electrons or ions and the partially enhanced plasma density structure based on energetic particles is distributed according to the change of the FAC direction. If the changes of the FACs are considerably small (a few kilometers in size), phase scintillation might occur. Although the asymmetry of small-scale FACs between the MLT dawn and dusk sectors has not been discussed in detail, it has been reported in previous studies (McGranaghan et al., 2017; Rother et al., 2007). A study of kilometer-scale FACs using high-resolution CHAMP measurements (50 Hz) revealed that the occurrence rates of strong kilometer-scale FACs in the MLT dawn sector are higher than those in the MLT dusk sector (see Figure 8 in Rother et al., 2007). Multiscale FACs were also compared using Swarm Level-2 FAC data; the results indicated higher amplitudes of small-scale FACs in the MLT dawn sector and symmetric large-scale FACs between the MLT dawn and dusk sectors (see Figure 15 in McGranaghan et al., 2017). Although the mechanism causing the asymmetry of small-scale FACs remains unclear, it might be the source of the phase scintillation asymmetry between the MLT dawn and dusk sectors. Phase scintillations more frequently occur in the L2 channel with lower signal frequency. It is known that the phase scintillation index anticorrelates with signal frequency such that σ_ϕ of the L2 channel theoretically is 1.28 times greater than that of the L1 channel (Kaplan & Hegarty, 2006). Although we statistically compared the results obtained for the L1 and L2 channels, higher occurrence rates of the L2 channel manifest the signal frequency dependencies.

5. Conclusions and Summary

We statistically analyzed the ionospheric scintillation indices of L-band GNSS signals recorded at a high-latitude single station in the Southern Hemisphere during a 2-year period (2017–2018). The occurrence rates of the ionospheric scintillation indices were computed and categorized according to the signal frequency type, geomagnetic conditions (K_p index), MLT, and season. Amplitude scintillations mostly occur at elevation angles below 30° . These might originate from ionospheric electron density irregularities or multipath contamination. However, it is hard to determine the actual source. We only considered elevation angles above 30° , which are considered to be ionospheric effects. Fluctuations of the electromagnetic waves intensity and phase penetrating the ionosphere can be expressed as a function of the inverse proportion of the signal frequency. Hence, higher occurrence rates are expected in the lower frequency channel (L2 channel in this case). However, there are no distinct amplitude scintillation occurrences at L2 as well. This means that the ionospheric irregularities smaller than the Fresnel radius are rarely created at high latitudes. In contrast, phase scintillations have various characteristics. The occurrence rates of phase scintillations show signal frequency dependency as expected that higher occurrence rates of the phase scintillation exist at the lower frequency channel (L2). The results show that ionospheric phase scintillations increase with geomagnetic disturbances, as generally expected. The occurrence rates of phase scintillations strongly correlate with the polar cusp, small-scale FACs, and the poleward edge of the auroral oval. Based on the

analysis of Swarm and DMSP data, the variations of ionospheric events over the JBS are similar to those of the observed occurrence rates of phase scintillations in terms of both the MLT and season, strongly suggesting that the polar cusp, FACs, and auroral activities significantly contribute to ionospheric scintillations. Because these phenomena depend on both the geomagnetic latitude and local time, ionospheric scintillations at high latitudes also strongly depend on the geomagnetic latitudes, in addition to the orientation relative to the geomagnetic pole. The phase scintillation characteristics over the JBS can be summarized as follows:

1. The phase scintillation occurrence rates are higher at lower frequency signals (L2 channel in this study), corresponding to the signal frequency dependency of the scintillation index.
2. The phase scintillation occurrence rates increase under geomagnetic disturbance, representing favorable conditions for the creation of ionospheric irregularities.
3. The occurrence rates of the phase scintillation are maximal (minimal) during the December solstices (June solstices), which is related to the seasonal dependencies of the polar cap patch, polar cusp, and FACs.
4. The MLT noon and dawn sectors exhibit higher occurrence rates. The asymmetries of small-scale FACs and the poleward edge of the auroral boundary cause the MLT dawn-dusk asymmetry of the phase scintillation.
5. Because of the location of the JBS, the number of phase scintillation occurrences is higher northeast of the JBS (absence southwest of the JBS).

Because this study is based on measurements of a single station, it is very similar to the environments of GNSS service users. Therefore, the results of this study provide guidelines for GNSS users regarding the degradation of the GNSS performance at high latitudes.

Data Availability Statement

The data set recorded at the JBS can be accessed online (at <https://kpsc.kopri.re.kr/>). Swarm satellite data are available on the website of the European Space Agency (ESA; <http://swarm-diss.eo.esa.int/>). The DMSP satellites data are available on the website of the National Centers for Environmental Information (NCEI) of the National Oceanic and Atmospheric Administration (NOAA; <https://satdat.ngdc.noaa.gov/dmsp/data/>).

Acknowledgments

This study was supported by a basic research fund from the Korea Astronomy and Space Science Institute (2020-1-8-5005) and by a research program of the Korea Polar Research Institute (PE20100). Y. H. K. acknowledges the support by a U.S. Air Force grant. The authors especially thank to the overwintering team at the Jang Bogo Station in Antarctica for their dedication to successful observations and maintenance. The work of H.-J. Kwon was supported by the Basic Science Research Program through 608 NRF funded by NRF-2020R1C1C1003640.

References

- Aarons, J. (1982). Global morphology of ionospheric scintillations. *Proceedings of the Institute of Electrical and Electronics Engineers*, 70(4), 360–378. <https://doi.org/10.1109/PROC.1982.12314>
- Aarons, J. (1997). Global Positioning System phase fluctuations at auroral latitudes. *Journal of Geophysical Research*, 102(A8), 17,219–17,231. <https://doi.org/10.1029/97JA01118>
- Basu, S., Basu, S., Chaturvedi, P. K., & Bryant, C. M. (1994). Irregularity structures in the cusp/cleft and polar cap regions. *Radio Science*, 29(1), 195–207. <https://doi.org/10.1029/93RS01515>
- Basu, S., Basu, S., MacKenzie, E., Coley, W. R., Sharber, J. R., & Hoegy, W. R. (1990). Plasma structuring by the gradient drift instability at high latitudes and comparison with velocity shear driven processes. *Journal of Geophysical Research*, 95(A6), 7799–7818. <https://doi.org/10.1029/JA095iA06p07799>
- Basu, S., Basu, S., Sojka, J. J., Schunk, R. W., & MacKenzie, E. (1995). Macroscale modeling and mesoscale observations of plasma density structures in the polar cap. *Geophysical Research Letters*, 22(8), 881–884. <https://doi.org/10.1029/95GL00467>
- Basu, S., & Groves, K. (2001). Specification and forecasting of outages on satellite communication and navigation systems. *AGU Space Weather Monograph*, 125, 423–430. <https://doi.org/10.1029/GM125p0423>
- Basu, S., Weber, E. J., Bullett, T. W., Keskinen, M. J., MacKenzie, E., Doherty, P., et al. (1998). Characteristics of plasma structuring in the cusp/cleft region at Svalbard. *Radio Science*, 33(6), 1885–1899. <https://doi.org/10.1029/98RS01597>
- Briggs, B. H., & Parkin, I. A. (1962). On the variation of radio star and satellite scintillations with zenith angle. *Journal of Atmospheric and Terrestrial Physics*, 25(6), 339–365. [https://doi.org/10.1016/0021-9169\(63\)90150-8](https://doi.org/10.1016/0021-9169(63)90150-8)
- Carlson, H. C., Oksavik, K., Moen, J., & Pedersen, T. (2004). Ionospheric patch formation: Direct measurements of the origin of a polar cap patch. *Geophysical Research Letters*, 31, L08806. <https://doi.org/10.1029/2003GL018166>
- Chartier, A. T., Mitchell, C. N., & Miller, E. S. (2018). Annual occurrence rates of ionospheric polar cap patches observed using Swarm. *Journal of Geophysical Research: Space Physics*, 123, 2327–2335. <https://doi.org/10.1002/2017JA024811>
- Clausen, L. B. N., Moen, J. I., Hosokawa, K., & Holmes, J. M. (2016). GPS scintillations in the high latitudes during periods of dayside and nightside reconnection. *Journal of Geophysical Research: Space Physics*, 121, 3293–3309. <https://doi.org/10.1002/2015JA022199>
- Crowley, G., Ridley, A. J., Deist, D., Wing, S., Knipp, D. J., Emery, B. A., et al. (2000). The transformation of high-latitude ionospheric F-region patches into blobs during the March 21, 1990 storm. *Journal of Geophysical Research*, 105(A3), 5215–5230. <https://doi.org/10.1029/1999JA900357>
- De Franceschi, G., Spogli, L., Alfonsi, L., Romano, V., Cesaroni, C., & Hunstad, I. (2019). The ionospheric irregularities climatology over Svalbard from solar cycle 23. *Scientific Reports*, 9(1), 9232. <https://doi.org/10.1038/s41598-019-44829-5>

- Drury, E. E., Mende, S. B., Frey, H. U., & Doolittle, J. H. (2003). Southern Hemisphere poleward moving auroral forms. *Journal of Geophysical Research*, *108*(A3), 1114. <https://doi.org/10.1029/2001JA007536>
- Forte, B. (2005). Optimum detrending of raw GPS data for scintillation measurements at auroral latitudes. *Journal of Atmospheric and Solar-Terrestrial Physics*, *67*(12), 1100–1109. <https://doi.org/10.1016/j.jastp.2005.01.011>
- Forte, B. (2007). On the relationship between the geometrical control of scintillation indices and the data detrending problems observed at high latitudes. *Annals of Geophysics*, *50*, 699–706. <https://doi.org/10.4401/ag-3051>
- Forte, B., & Radicella, S. M. (2002). Problems in data treatment for ionospheric scintillation measurements. *Radio Science*, *37*, 1096. <https://doi.org/10.1029/2001RS002508>
- Foster, J. C., Coster, A. J., Erickson, P. J., Holt, J. M., Lind, F. D., Rideout, W., et al. (2005). Multiradar observations of the polar tongue of ionization. *Journal of Geophysical Research*, *110*, A09S31. <https://doi.org/10.1029/2004JA010928>
- Fremouw, E. J., Leadabrand, R. L., Livingston, R. C., Cousins, M. D., Rino, C. L., Fair, B. C., & Long, R. A. (1978). Early results from the DNA wideband satellite experiment—Complex-signal scintillation. *Radio Science*, *13*(1), 167–187. <https://doi.org/10.1029/RS013i001p00167>
- Friis-Christensen, E., Lühr, H., Knudsen, D., & Haagmans, R. (2008). Swarm—An Earth observation mission investigating geospace. *Advances in Space Research*, *41*(1), 210–216. <https://doi.org/10.1016/j.asr.2006.10.008>
- Goodwin, L. V., Iserhienrhien, B., Miles, D. M., Patra, S., van der Meer, C., Buchert, S. C., et al. (2015). Swarm in situ observations of *F* region polar cap patches created by cusp precipitation. *Geophysical Research Letters*, *42*, 996–1003. <https://doi.org/10.1002/2014GL026210>
- Heikkila, W. J., & Winningham, J. D. (1971). Penetration of magnetosheath plasma to low altitudes through the dayside magnetospheric cusps. *Journal of Geophysical Research*, *76*(4), 883–891. <https://doi.org/10.1029/JA076i004p00883>
- Jiao, Y., Morton, Y. T., Taylor, S., & Pelgrum, W. (2013). Characterization of high-latitude ionospheric scintillation of GPS signals. *Radio Science*, *48*, 698–708. <https://doi.org/10.1002/2013RS0>
- Jin, Y., Moen, J. I., & Miloch, W. J. (2014). GPS scintillation effects associated with polar cap patches and substorm auroral activity: Direct comparison. *Journal of Space Weather Space Climatology*, *4*. <https://doi.org/10.1051/swsc/2014019>
- Jin, Y., Moen, J. I., & Miloch, W. J. (2015). On the collocation of the cusp aurora and the GPS phase scintillation: A statistical study. *Journal of Geophysical Research: Space Physics*, *120*, 9176–9191. <https://doi.org/10.1002/2015JA021449>
- Jin, Y., Moen, J. I., Oksavik, K., Spicher, A., Clausen, L. B. N., & Miloch, W. J. (2017). GPS scintillations associated with cusp dynamics and polar cap patches. *Journal of Space Weather Space Climatology*, *7*. <https://doi.org/10.1051/swsc/2017022>
- Kaplan, E. D. & Hegarty, C. J. (2006). *Understanding GPS: Principles and applications* second edition, Artech House. ISBN-10: 1-58053-894-0
- Kelley, M. C., Vickrey, J. F., Carlson, C. W., & Torbert, R. (1982). On the origin and spatial extent of high-latitude *F* region irregularities. *Journal of Geophysical Research*, *87*(A6), 4469–4475. <https://doi.org/10.1029/JA087iA06p04469>
- Kinrade, J., Mitchell, C. N., Smith, N. D., Ebihara, Y., Weatherwax, A. T., & Bust, G. S. (2013). GPS phase scintillation associated with optical auroral emissions: First statistical results from the geographic South Pole. *Journal of Geophysical Research: Space Physics*, *118*, 2490–2502. <https://doi.org/10.1002/jgra.50214>
- Kinrade, J., Mitchell, C. N., Yin, P., Smith, N., Jarvis, M. J., Maxfield, D. J., et al. (2012). Ionospheric scintillation over Antarctica during the storm of 5–6 April 2010. *Journal of Geophysical Research*, *117*, A05304. <https://doi.org/10.1029/2011JA017073>
- Kintner, P. M., Ledvina, B. M., & de Paula, E. R. (2007). GPS and ionospheric scintillations. *Space Weather*, *5*, S09003. <https://doi.org/10.1029/2006SW000260>
- Knudsen, W. C., Banks, P. M., Winningham, J. D., & Klumpkor, D. M. (1977). Numerical model of the convecting *F2* ionosphere at high latitudes. *Journal of Geophysical Research*, *82*(4784), 1977–4792. <https://doi.org/10.1029/JA082i029p04784>
- Li, G., Ning, B., Ren, Z., & Hu, L. (2010). Statistics of GPS ionospheric scintillation and irregularities over polar regions at solar minimum. *GPS Solutions*, *14*(4), 331–341. <https://doi.org/10.1007/s10291-009-0156-x>
- McCaffrey, A. M., & Jayachandran, P. T. (2019). Determination of the refractive contribution to GPS phase “scintillation”. *Journal of Geophysical Research: Space Physics*, *124*, 1454–1469. <https://doi.org/10.1029/2018JA025759>
- McGranaghan, R. M., Mannucci, A. J., & Forsyth, C. (2017). A comprehensive analysis of multiscale field-aligned currents: Characteristics, controlling parameters, and relationships. *Journal of Geophysical Research: Space Physics*, *122*, 11,931–11,960. <https://doi.org/10.1002/2017JA024742>
- Mushini, S. C., Jayachandran, P. T., Langley, R. B., MacDougall, J. W., & Pokhotelov, D. (2012). Improved amplitude- and phase-scintillation indices derived from wavelet detrended high-latitude GPS data. *GPS Solutions*, *16*(3), 363–373. <https://doi.org/10.1007/s10291-011-0238-4>
- Newell, P. T., & Meng, C. I. (1988). The cusp and the cleft/boundary layer: Low-altitude identification and statistical local time variation. *Journal of Geophysical Research*, *93*(A12), 14,549–14,556. <https://doi.org/10.1029/JA093iA12p14549>
- Nichols, D. A. (1976). *DMSP Block-5A, B, C Compendium*, Space Division/YDE. Los Angeles, Calif: U.S. Air Force, Weather Service.
- Noja, M., Stolle, C., Park, J., & Lühr, H. (2013). Long-term analysis of ionospheric polar patches based on CHAMPTEC data. *Radio Science*, *48*, 289–301. <https://doi.org/10.1002/rds.20033>
- Oksavik, K., Van der Meer, C., Lorentzen, D. A., Baddeley, L. J., & Moen, J. (2015). Scintillation and loss of signal lock from poleward moving auroral forms in the cusp ionosphere. *Journal of Geophysical Research: Space Physics*, *120*, 9161–9175. <https://doi.org/10.1002/2015JA021528>
- Park, J., Ehrlich, R., Lühr, H., & Ritter, P. (2012). Plasma irregularities in the high-latitude ionospheric *F*-region & their diamagnetic signatures as observed by CHAMP. *Journal of Geophysical Research*, *117*, A10322. <https://doi.org/10.1029/2012JA018166>
- Prikryl, P., Jayachandran, P. T., Chadwick, R., & Kelly, T. D. (2015). Climatology of GPS phase scintillation at northern high latitudes for the period from 2008 to 2013. *Annales Geophysicae*, *33*(5), 531–545. <https://doi.org/10.5194/angeo-33-531-2015>
- Prikryl, P., Jayachandran, P. T., Mushini, S. C., Pokhotelov, D., MacDougall, J. W., Donovan, E., et al. (2010). GPS TEC, scintillation and cycle slips observed at high latitudes during solar minimum. *Annales Geophysicae*, *28*(6), 1307–1326. <https://doi.org/10.5194/angeo-28-1307-2010>
- Priyadarshi, S., & Wernik, A. W. (2013). Variation of the ionospheric scintillation index with elevation angle of the transmitter. *Acta Geophysica*, *61*(5), 1279–1288. <https://doi.org/10.2478/s11600-013-0123-3>
- Rino, C. L. (1979). A power law phase screen model for ionospheric scintillation: 1. Weak scatter. *Radio Science*, *14*(6), 1135–1145. <https://doi.org/10.1029/RS014i006p01135>
- Ritter, P., Lühr, H., & Rauberg, J. (2013). Determining field-aligned currents with the Swarm constellation mission. *Earth, Planets and Space*, *65*(11), 1285–1294. <https://doi.org/10.5047/eps.2013.09.006>

- Rother, M., Schlegel, K., & Lühr, H. (2007). CHAMP observation of intense kilometer-scale field-aligned currents, evidence for an ionospheric Alfvén resonator. *Annales Geophysicae*, *25*(7), 1603–1615. <https://doi.org/10.5194/angeo-25-1603-2007>
- Ruohoniemi, J. M., Greenwald, R. A., Baker, K. B., Villain, J. P., & McCready, M. A. (1987). Drift motions of small-scale irregularities in the high-latitude *F* region: An experimental comparison with plasma drift motions. *Journal of Geophysical Research*, *92*(A5), 4553–4564. <https://doi.org/10.1029/JA092iA05p04553>
- Secan, J. A., Bussey, R. M., Fremouw, E. J., & Basu, S. (1997). High latitude upgrade to the Wideband ionospheric scintillation model. *Radio Science*, *32*(4), 1567–1574. <https://doi.org/10.1029/97RS00453>
- Smith, A., Pryse, S., & Kersley, L. (2000). Polar patches observed by ESR and their possible origin in the cusp region. *Annales Geophysicae*, *18*(9), 1043–1053. <https://doi.org/10.1007/s00585-000-1043-5>
- Sojka, J. J., Bowline, M. D., Schunk, R. W., Decker, D. T., Valladares, C. E., Sheehan, R., et al. (1993). Modeling polar cap *F* region patches using time varying convection. *Geophysical Research Letters*, *20*(17), 1783–1786. <https://doi.org/10.1029/93GL01347>
- Sojka, J. J., Subramaniam, M. V., Zhu, L., & Schunk, R. W. (1998). Gradient drift instability growth rates from global-scale modeling of the polar ionosphere. *Radio Science*, *33*(6), 1915–1928. <https://doi.org/10.1029/98RS02490>
- Spicher, A., Clausen, L. B. N., Miloch, W. J., Lofstad, V., Jin, Y., & Moen, J. I. (2017). Interhemispheric study of polar cap patch occurrence based on Swarm in situ data. *Journal of Geophysical Research: Space Physics*, *122*, 3837–3851. <https://doi.org/10.1002/2016JA023750>
- Spicher, A., Deshpande, K., Jin, Y., Oksavik, K., Zettergren, M. D., Clausen, L. B. N., et al. (2020). On the production of ionospheric irregularities via Kelvin-Helmholtz instability associated with cusp flow channels. *Journal of Geophysical Research: Space Physics*, *125*, e2019JA027734. <https://doi.org/10.1029/2019JA027734>
- Spogli, L., Alfonsi, L., De Franceschi, G., Romano, V., Aquino, M. H. O., & Dodson, A. (2009). Climatology of GPS ionospheric scintillations over high and mid-latitude European regions. *Annales Geophysicae*, *27*(9), 3429–3437. <https://doi.org/10.5194/angeo-27-3429-2009>
- Tsunoda, R. T. (1988). High-latitude *F* region irregularities: A review and synthesis. *Reviews of Geophysics*, *26*(4), 719–760. <https://doi.org/10.1029/RG026i004p00719>
- Valladares, C. E., Basu, S., Buchau, J., & Friis-Christensen, E. (1994). Experimental evidence for the formation and entry of patches into the polar cap. *Radio Science*, *29*(1), 167–194. <https://doi.org/10.1029/93RS01579>
- Van der Meeren, C., Oksavik, K., Lorentzen, D., Moen, J. I., & Romano, V. (2014). GPS scintillation and irregularities at the front of an ionization tongue in the nightside polar ionosphere. *Journal of Geophysical Research: Space Physics*, *119*, 8624–8636. <https://doi.org/10.1002/2014JA020114>
- Van der Meeren, C., Oksavik, K., Lorentzen, D. A., Rietveld, M. T., & Clausen, L. B. N. (2015). Severe and localized GNSS scintillation at the poleward edge of the nightside auroral oval during intense sub-storm aurora. *Journal of Geophysical Research: Space Physics*, *120*, 10,607–10,621. <https://doi.org/10.1002/2015JA021819>
- Voss, H. D., & Smith, L. G. (1979). Nighttime ionization by energetic particles at Wallops Island in the altitude region 120 to 200 km. *Geophysical Research Letters*, *6*(2), 93–96. <https://doi.org/10.1029/GL006i002p00093>
- Walker, I., Moen, J., Kersley, L., & Lorentzen, D. (1999). On the possible role of cusp/cleft precipitation in the formation of polar-cap patches. *Annales Geophysicae*, *17*(10), 1298–1305. <https://doi.org/10.1007/s00585-999-1298-4>
- Wang, Y., Zhang, Q. H., Jayachandran, P. T., Lockwood, M., Zhang, S. R., Moen, J., et al. (2016). A comparison between large-scale irregularities and scintillations in the polar ionosphere. *Geophysical Research Letters*, *43*, 4790–4798. <https://doi.org/10.1002/2016GL069230>
- Weber, E. J., Klobuchar, J. A., Buchau, J., & Carlson, H. C. (1986). Polar cap *F* layer patches: Structure and Dynamics. *Journal of Geophysical Research*, *91*(A11), 12,121–12,120. <https://doi.org/10.1029/JA091iA11p12121>
- Wernik, A. W., Alfonsi, L., & Materassi, M. (2007). Scintillation modeling using in situ data. *Radio Science*, *42*, RS1002. <https://doi.org/10.1029/2006RS003512>
- Xiong, C., Lühr, H., Wang, H., & Johnsen, M. G. (2014). Determining the boundaries of the auroral oval from CHAMP field-aligned current signatures—Part 1. *Annales Geophysicae*, *32*(6), 609–622. <https://doi.org/10.5194/angeo-32-609-2014>
- Yeh, K. C., & Liu, C. H. (1982). Radio wave scintillations in the ionosphere. *Proceedings of the IEEE*, *70*, 324–360.
- Zhang, Q. H., Zhang, B. C., Moen, J., Lockwood, M., McCrea, I. W., Yang, H. G., et al. (2013). Polar cap patch segmentation of the tongue of ionization in the morning convection cell. *Geophysical Research Letters*, *40*, 2918–2922. <https://doi.org/10.1002/grl.50616>